Numerical simulations of crack formation from pegs in thermal barrier systems with NiCoCrAlY bond coats

H.X. Zhu [a], N.A. Fleck [a,*], A.C.F. Cocks [b], A.G. Evans [c]

[a] *Department of Engineering, University of Cambridge, Trumpington Street, Cambridge CB2 1PZ, UK*
[b] *Department of Engineering, University of Leicester, Leicester LE1 7RH, UK*
[c] *Materials and Mechanical Engineering Departments, University of California, Santa Barbara, CA 93106, USA*

Abstract

The high temperature exposure of thermal barrier systems with MCrAlY bond coats is accompanied by non-uniform thickening of the thermally grown oxide (TGO). The heterogeneities are manifest as intrusions into the bond coat, referred to as "pegs". The progressive growth and swelling of these intrusions, in conjunction with the thermal expansion mismatch from layer to layer, leads to the development of localized strains upon thermal cycling. A finite element study reports on the evolution of the stress state and of the plastic strains in the vicinity of the pegs, and on the conditions under which cracks may initiate and advance. It is demonstrated that large plastic strains accumulate near the peg. Moreover, large shear stresses arise that could motivate mode II (shear) cracking along the interface between the bond coat and thermally grown oxide. However, for realistic sizes of peg, the energy release rate is always much less than the interface toughness. It is concluded that the pegs do not behave as imperfections that initiate cracks, but rather, serve a beneficial purpose of fastening the TGO to the bond coat.

1. Introduction

Multi-layer thermal barrier systems are commonly used in gas turbines for propulsion and power generation [1–4]. The systems are susceptible to performance degradation when the outermost thermal barrier layer, typically yttria-stabilized-zirconia (YSZ), experiences local spalling. One category of failure mechanism is associated with the stresses and displacements due to the misfit between the thermally grown oxide (TGO) and the other layers. These stresses cause cracks to nucleate and propagate as the system experiences thermal cycling [5–11]. The specifics are system-dependent. The most detailed understanding has been developed for systems comprising electron beam deposited (EB-PVD) thermal barrier coatings (TBCs) with β-phase, Pt–aluminide bond coats [4–11]. In such systems, the TGO develops displacement

instabilities enabled by elongation of the TGO as it thickens. Models of this mechanism have been developed [12,13], validated by experiment [14,15], and used to relate the durability to constituent properties [12].

In systems comprising a two-phase (β, γ′) NiCrAlY bond coat with an EB-PVD TBC, a different TGO-based failure mechanism applies [10,16]. The TGO develops thickness heterogeneities (often referred to as "pegs"), which contain oxides other than alumina, such as the Y(Hf)O$_2$ fluorite [16] (Fig. 1). Delamination occurs primarily along the interface between the TGO and the bond coat [16]. The cracks extend through the TGO only at the locations of the "pegs". They do not enter into the TBC layer. The overall influence of the "pegs" on durability is unresolved, because of two countervailing effects [16]: (a) they might adversely affect failure by acting as local stress intensification sites at the interface and (b) they could behave as obstacles that impede the extension of interface cracks. The present analysis will address the first topic.

* Corresponding author. Tel.: +44 1223 332650; fax: +44 1223 765046.
E-mail address: NAF1@eng.cam.ac.uk (N.A. Fleck).
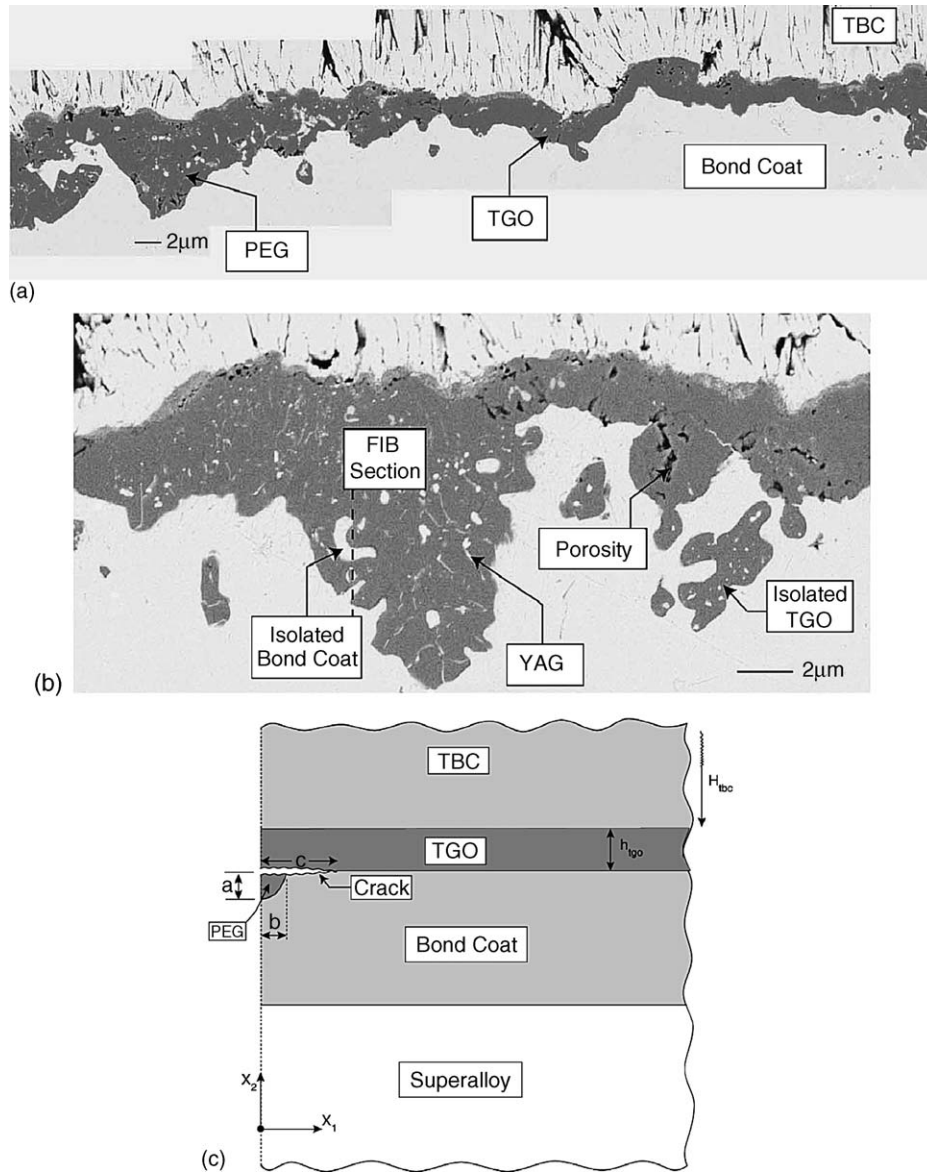
Fig. 1. (a and b) Cross-sections of pegs in a TBC system with NiCoCrAlY bond coat [16] and (c) sketch of an ellipsoidal peg growing into the bond coat. The most likely crack location is included.

The outline is as follows. The stress state in the vicinity of a peg is obtained for two types of loading: thermal expansion mismatch and TGO growth. The stress evolution with increasing number of thermal cycles is obtained and the sensitivity of these stresses to the geometry of the peg is ascertained. A fracture mechanics analysis is performed to determine the conditions under which a crack might initiate and grow.

2. Constituent properties

The thermo-elastic properties of the layers are presented in Table 1. Creep occurs in all three constituents of the coat-ing at the highest temperatures in the thermal cycle. The modeling challenge is to incorporate creep representations with sufficiently small times per computation so that trends in the response can be predicted with reasonable fidelity. Two approaches have been pursued in the literature. One is

Table 1
The thermo-elastic properties of the layers

Material	Young's modulus, E (GPa)	Poisson ratio, ν	Thermal expansion coefficient, α (10^{-6} K^{-1})
TBC	40	0.3	11
TGO	370	1/6	8
Bond coat	210	1/3	15
Substrate	210	1/3	15
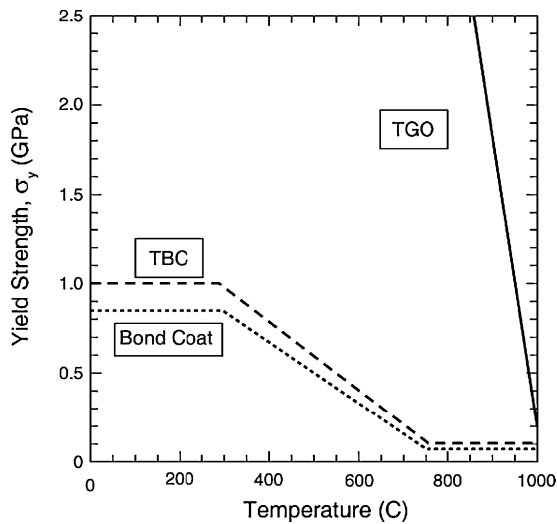
Fig. 2. The temperature-dependent yield strengths of the bond coat (BC), thermally grown oxide (TGO), and the thermal barrier coating (TBC). The nickel alloy substrate is taken to be elastic.

Fig. 3. Growth stresses measured in situ using a synchotron for thermally grown alumina forming on Pt–aluminide [20]. The growth stress is indicated as well as the thermo-elastic stress changes caused by thermal expansion misfit upon heating and cooling.

based on a special purpose analytic code that allows constituent creep to be incorporated [13] (using independently measured power law creep data [17]). The other, which uses the commercial finite element code ABAQUS [7,12], regards the constituents as elastic/perfectly plastic with flow stress given by the creep strength at representative strain-rates. This strength is found from independent tests conducted at constant strain-rate in a range consistent with the misfit imposed by the growing TGO. The deformation to be incorporated is a temperature-dependent flow strength. The justifications for this approach are based on comparisons with results generated by the creep model [13] and with experimental measurements [14,15]. For the NiCoCrAlY bond coat, the temperature dependence of the strength is obtained from a turbine industry source [18] (Fig. 2).

Incorporating the deformation of the TGO requires additional considerations [7,12,13]. In most cases, the TGO elongates at temperature (because of internal formation [7,19]), with associated lateral strain-rate, causing the TGO to be in compression during growth. The compressive stress remains constant during growth (Fig. 3) at a level dictated by its creep strength [20]. This growth stress differs among TGOs formed on different alloys indicative of different creep characteristics. When pre-oxidized to form α-Al$_2$O$_3$ a few micrometres in thickness, the following growth stresses have been measured: (a) -1000 ± 100 MPa for FeCrAlY, (b) -200 ± 100 MPa for Pt–aluminide, and (c) -50 ± 50 MPa for NiCoCrAlY. Here, we adopt the worst case scenario for NiCoCrAlY by assuming a relatively high compressive growth stress ($\sigma_Y^{\text{tgo}} \approx -200$ MPa) similar to that found in Pt–aluminide systems [20]. Our intention is to explore whether the stresses so generated in the vicinity of pegs can be sufficiently large to produce cracking. On cooling/reheating, at lower temperature, the TGO layer becomes elastic (Fig. 2).
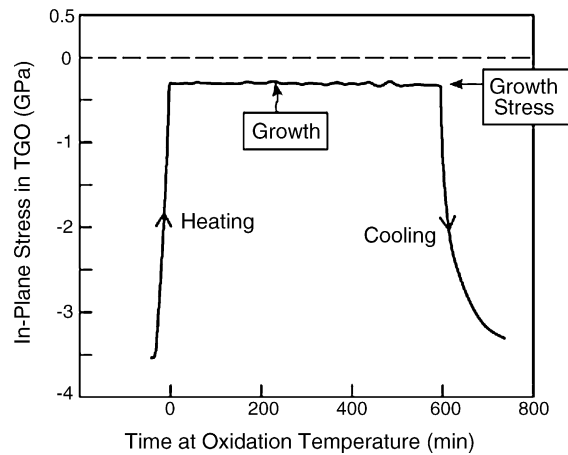
A suitable behavior for the peg must be incorporated. Since its growth involves the internal formation of Y(Hf)O$_2$, while also entraining bond coat [16], it is considered to expand volumetrically. This effect is captured in the model by imposing a relatively large volumetric strain. The actual value is not especially important because the deformation is accommodated by the deformation of the bond coat and TGO. In practice, it is assumed that $\varepsilon_{11} = \varepsilon_{22} = \varepsilon_{33} = 0.025$ per cycle within the peg, consistent with the measured growth rates.

Observations of delaminations at the TGO/bond coat interface in NiCoCrAlY systems indicate that they form at low temperature, usually during cooling [16]. Consequently, the cracks develop within a residual stress field induced by prior thermal cycling. Moreover, the system is essentially elastic during cracking, subject to a relatively low crack opening displacement, with no attendant plasticity [16]. Again, by using elastic concepts of fracture, the worst case scenario is envisaged, since the presence of plasticity local to the crack would reduce the energy release rate.

3. Finite element model

The peg is regarded as an isolated, semi-ellipsoidal domain consisting of TGO (Fig. 1c). Unless otherwise stated, the following ratios are taken as representative: peg depth to TGO thickness, $a/h_{\text{tgo}} = 1/2$; aspect ratio, $b/a = 2/3$. The thermal barrier coating thickness $H_{\text{tbc}}/h_{\text{tgo}} = 50$ equals that of the bond coat, $H_{\text{bc}}/h_{\text{tgo}} = 50$. The underlying superalloy substrate is taken to be sufficiently thick (1000 times the TGO thickness) to behave as a half-space. Since the bond coat shares the same elastic properties as the substrate and the plastic zone within the bond coat does not reach the bond coat/substrate interface, the precise value of bond coat thickness is unimportant.

The finite element analysis was performed using ABAQUS Standard. A mesh sensitivity study revealed that
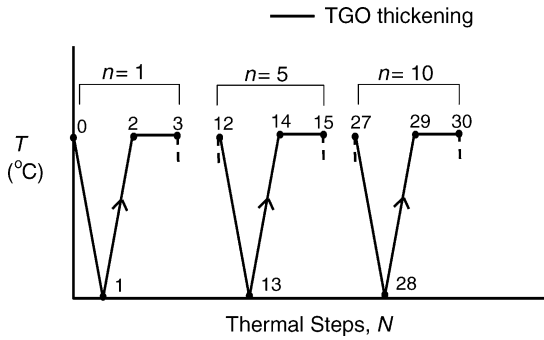
Fig. 4. The assumed thermal loading history. The n thermal cycles are subdivided into N steps.

adequate accuracy was achieved using about 20,000 quadrilateral elements (CAX4R) and 20,000 nodes. A cylindrical co-ordinate system is adopted for the axisymmetric model with x_1 as the radial co-ordinate and x_2 as the axial co-ordinate (see Fig. 1c). The boundary conditions are as follows. Along the axis of symmetry, $u_1 = 0$, while along the bottom of the mesh, $u_2 = 0$. The radial extent of the mesh L is typically

Fig. 5. (a) Contours of von Mises plastic strain ε_{pl} after $N = 30$ thermal steps and (b) progressive enlargement of the plastic zone, as characterised by the contour $\varepsilon_{pl} = 0.001$, with increasing number N of thermal steps.

1000a, and along the outer boundary, $x_1 = L$. The radial displacements $u_1(L)$ are constrained to be uniform, with zero net radial force.

In the first part of this study, the evolution of stress state is determined in the vicinity of the peg, absent cracking. The possibility of cracking is also addressed, with the most likely location of a penny-shaped crack of radius c shown in Fig. 1c. The stresses are largest, and the interfacial toughness between bond coat and TGO is least at ambient temperature. Simplified finite element calculations are performed to assess the likelihood of cracking: it is envisaged that a putative penny-shaped crack is loaded by the residual stress state, and the energy release rate is calculated.

The thermal loading history is sketched in Fig. 4, and is taken to be spatially uniform. Initially, the TBC system is taken to be stress-free at the peak temperature (1000 °C). The TGO is allowed to grow at this temperature by imposing stress-free strains in accordance with a user material subroutine [9]. As remarked above, the peg is considered to expand volumetrically by imposing a relatively large growth strain, $\varepsilon_{11} = \varepsilon_{22} = \varepsilon_{33} = 0.025$ per cycle. Due to computational limitations, a maximum of 30 thermal steps is considered.

4. Stress and strain states near a peg

4.1. Plastic zone development

The pegs "indent" both the bond coat and the overlaying TBC layer causing them to deform plastically. The distribution of von Mises effective plastic strain ε_{pl} (Fig. 5a) indicates that the plastic zones within the TBC and bond coat progressively enlarge due to the accumulation of growth strain (Fig. 5b). The zone shape remains approximately hemispherical in both the bond coat and TBC.
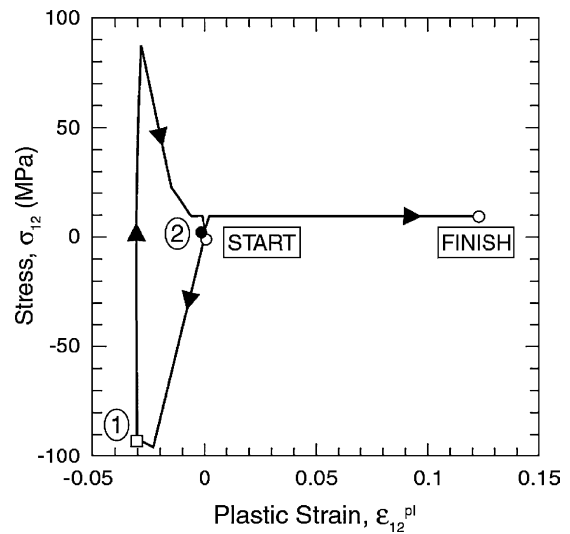
Fig. 6. Shear stress/strain response of the bond coat. For clarity, only the first stress–strain loop is shown (with thermal steps 1 and 2 marked), as well as the strain component ε_{12} at the end of the high temperature hold.

Examination of the stress–strain history reveals that the largest strain component, ε_{12}, increases cycle-by-cycle with the accumulation of growth strain in the TGO (Fig. 6). The strain hysteresis upon temperature cycling demonstrates that the thermal expansion mismatch induces cyclic plasticity. Such effects could be a source of fatigue.

4.2. Traction distribution between the TGO and BC

Calculations of the traction distribution (σ_{12}, σ_{22}) along the plane A–A′ (Fig. 5a) have been used to inform the subsequent assessment of cracks. The tractions normal to the plane of potential cracking are compressive within and adjacent to the peg (Fig. 7a and b). Such stresses inhibit cracking. However, large shear stresses also develop after cool-down (Fig. 7c), implying that cracks traversing the peg develop a (mode II) energy release rate. Outside the peg, the shear

stresses change sign, indicative of crack confinement [21]. The consequences become apparent when the energy release rates are evaluated below. Further calculations have revealed the following:

(i) The tractions are greatest at ambient temperature. Independent calculations of the tractions from the two sources of stress (thermal expansion mismatch and peg growth) reveal that the thermal expansion mismatch dominates.

(ii) Simulations in which the growth strain per cycle has been varied have indicated that the traction distribution is minimally affected by cycling, enabling it to be adequately expressed in terms of the total accumulated growth strain. Consequently, the precise value of growth strain per cycle is of limited significance.

The effects of peg size and shape upon the traction along plane A–A′ have been explored by two additional sets of
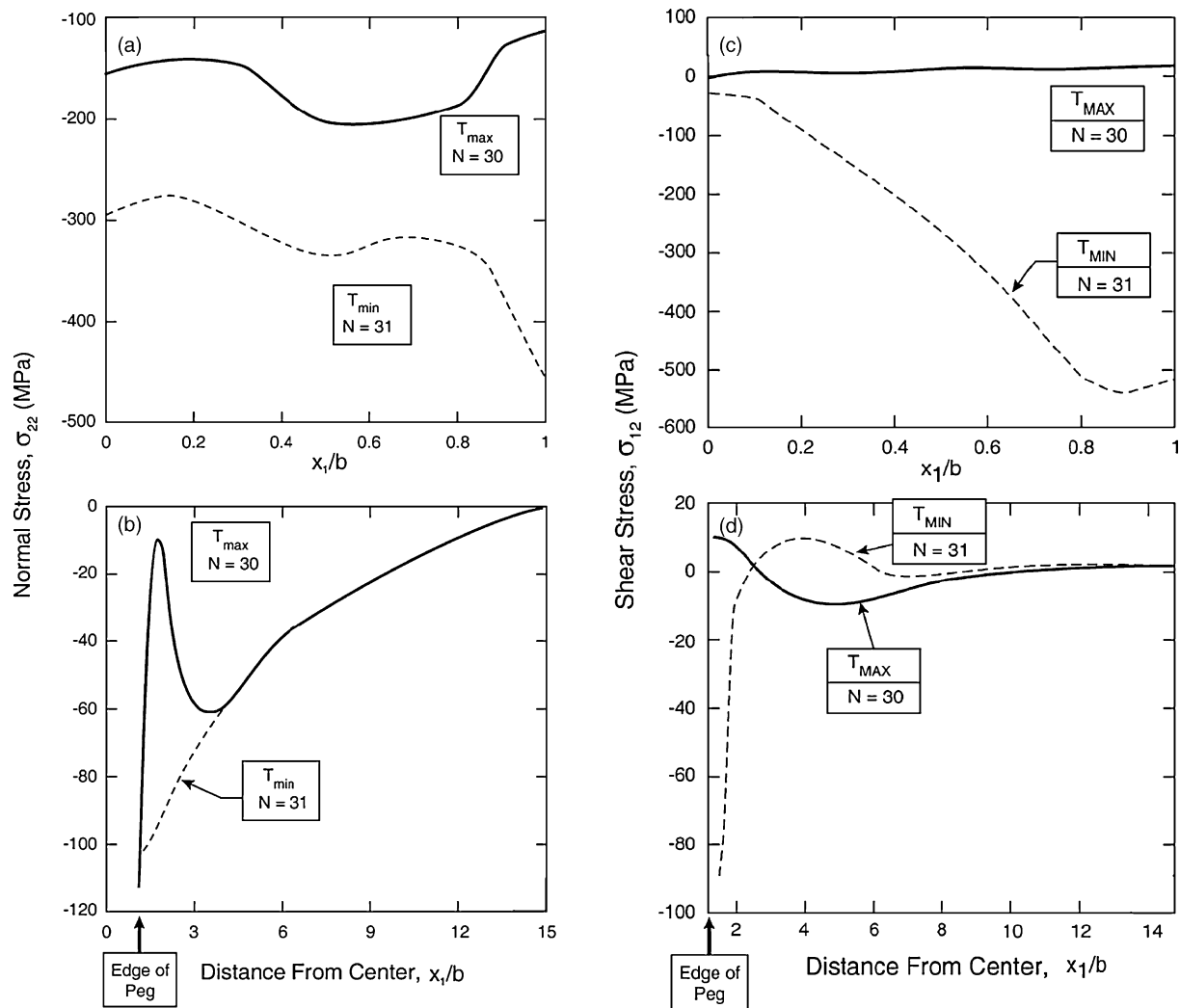
Fig. 7. The normal and shear tractions on the plane A–A′ defined in Fig. 5a. The tractions are shown after 10 thermal cycles at the end of the high temperature hold ($N = 30$) and after cool-down ($N = 31$). (a) Normal traction on plane within the peg, $x < b$; (b) normal traction on the TGO/bond coat interface beyond the peg, $x > b$; (c) shear traction on plane within the peg, $x < b$; (d) shear traction on the TGO/bond coat interface beyond the peg, $x > b$. Note that the normal stresses are discontinuous at the peg.
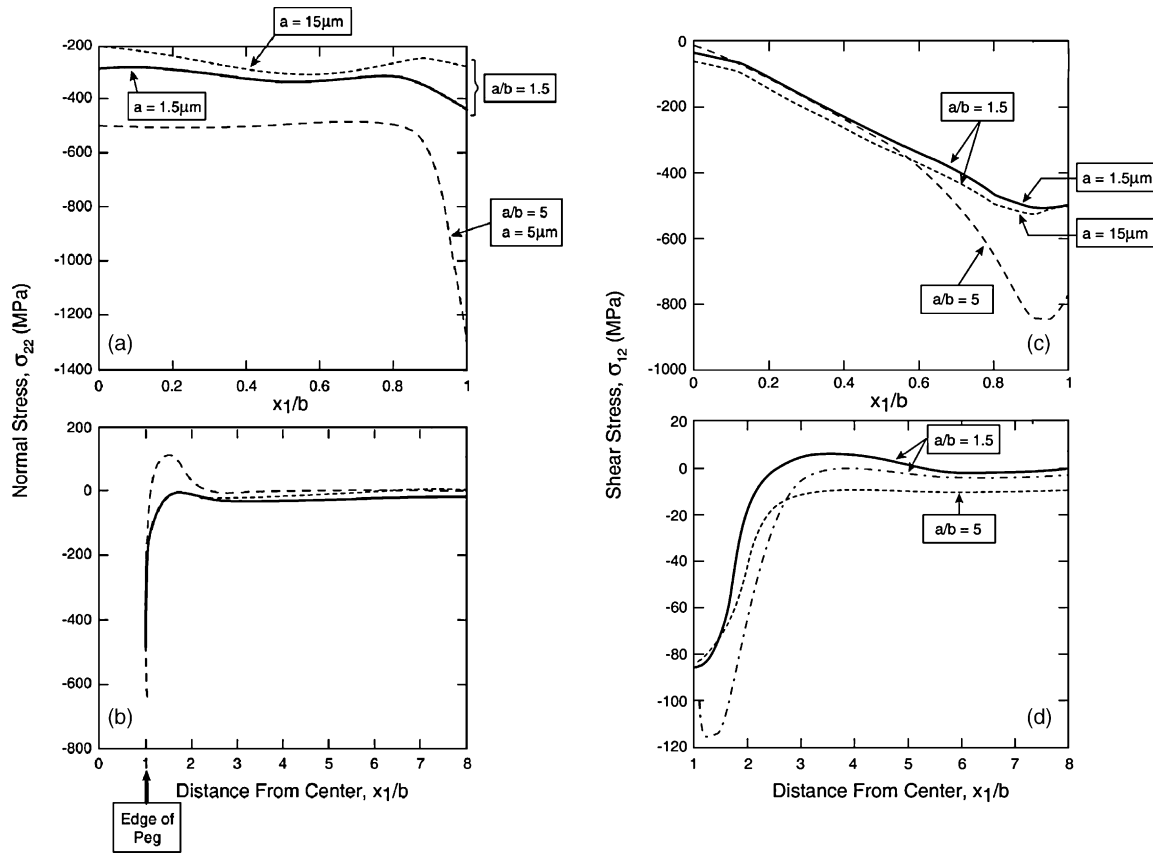
Fig. 8. The effects of peg size and shape on the normal and shear tractions on plane A–A′, as defined in Fig. 5a. The tractions are shown after 10 thermal cycles after cool-down ($N = 31$). (a) Traction on plane within the peg, $x_1 < b$; (b) traction on the TGO/bond coat interface beyond the peg, $x_1 > b$; (c) shear traction on plane within the peg, $x_1 < b$; (d) shear traction on the TGO/bond coat interface beyond the peg, $x_1 > b$.

calculations. One has examined pegs geometrically similar but 10 times larger ($a/h_{tgo} = 5$, $a/b = 1.5$). The other considers pegs with the same minor axis, but 10/3 times longer ($a/h_{tgo} = 5/3$, $a/b = 5$). The results (Fig. 8) demonstrate that the increase in size has essentially no effect upon the stress. In contrast, an increase in the aspect ratio leads to an increase in both the shear and normal tractions.

A preliminary sensitivity analysis has revealed that the shear stress within the peg scales linearly with the strength of the TGO material, but is much less sensitive to the strength of the bond coat.

5. Crack formation

Cracks can form within the residual stress field, and extend along the interface outside the peg as well as through the TGO internal to the peg (Fig. 1). In order to explore the likelihood of such cracking, it is imagined that a circular penny-shaped crack, radius c, develops along the adjacent interface, with its centre coincident with the axis of the peg, as sketched in Fig. 1c. The energy release rate J and mode-mix have been determined. To simplify the interpretation of the mode-mix, the Young's modulus and Poisson ratio of the TGO and bond coat are chosen to ensure that the Dundurs' parameter $\beta = 0$ [22,23].

Sets of calculations have been performed for a peg with fixed aspect ratio ($a = 1.5b$), but various sizes ($b = 1$, 3, 10 and 30 μm). The crack was introduced with $0 < c < 10b$. Wherever the crack faces make contact, a Coulomb friction coefficient is imposed (with $\mu = 0$, 0.3 and 0.6). The crack is modeled by gap elements, with negligible initial opening. Since the system is elastic at ambient temperature, when the cracks form, the J-integral can be calculated by the nodal release method within the finite element code, ABAQUS. Typical results (Fig. 9a) indicate that J has a characteristic variation with crack length, starting at zero, increasing to a peak J_{max} (at $c = b$), and then decreasingly rapidly with further increase in crack length, attributed to the change in the sign of the shear stress. Because of the normal compression, the crack is mode II throughout. The peak J_{max} increases linearly with increase in peg size (Fig. 9b), with magnitude strongly dependent on the level of friction. However, even for the largest pegs and the lowest friction, the J-values are less than the typical value of interfacial toughness, 20 J m^{-2} [24]. Consequently, the likelihood of cracks forming at pegs is minimal, unless the interface has been severely embrittled (for example, by the segregation of S) [25].
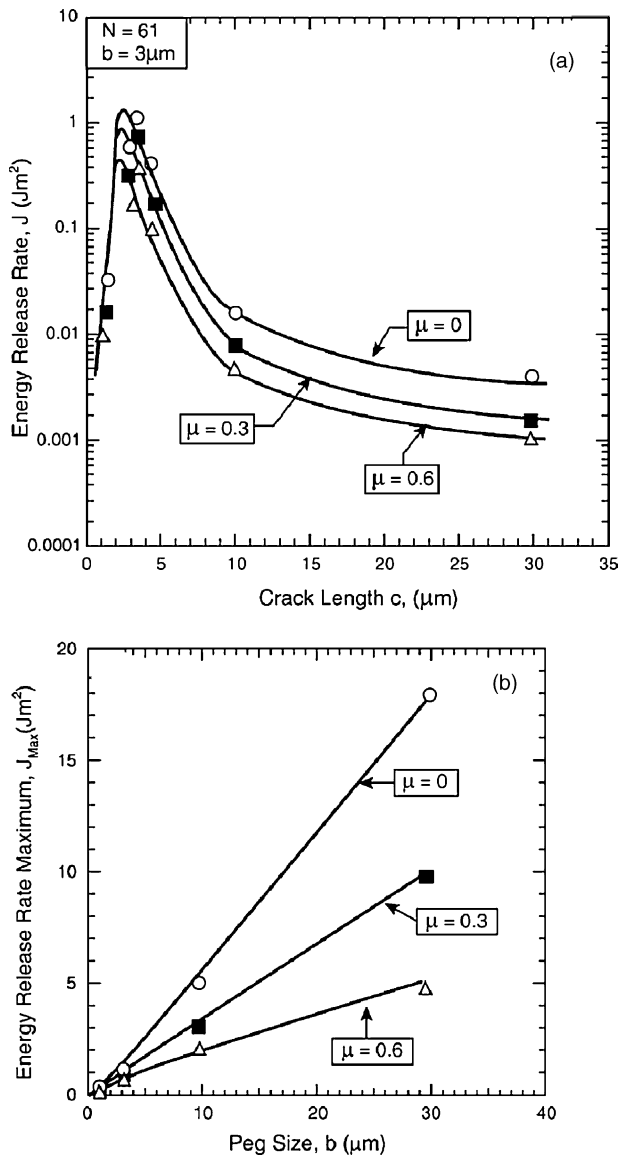
Fig. 9. Calculation of J after 10 thermal cycles after cool-down ($N = 31$). (a) Effect of crack radius c upon the mode II J-integral, for a peg of dimension $a = 4.5\,\mu m$, $b = 3\,\mu m$, and (b) plot of the maximum value of J with respect to crack radius c plotted against peg size, b.

6. Conclusion

A finite element study has reported on the evolution of the stress state and of the plastic strains in the vicinity of the pegs, and on the conditions under which cracks may initiate and advance. The results have been used to explore whether a penny-shaped crack centred on the peg will be created by thermal loading. It is concluded that the magnitude of energy release rate is too small to form a crack unless the peg is unrealistically large (requiring a radius greater than 30 μm). Thus, pegs may serve more of a protective role in fastening the TGO layer to the underlying bond coat rather than promoting interfacial separation.

References

[1] R.G. Wellman, J.R. Nicholls, Wear 242 (2000) 89–96.
[2] A.G. Evans, D.R. Mumm, J.W. Hutchinson, G.H. Meier, F.S. Pettit, Prog. Mater. Sci. 46 (2001) 505–553.
[3] R.A. Miller, J. Am. Ceram. Soc. 67 (1984) 517–521.
[4] P.K. Wright, Mater. Sci. Eng. A245 (1998) 191–200.
[5] D.R. Mumm, A.G. Evans, I.T. Spitsberg, Acta Mater. 49 (2001) 2329–2340.
[6] J.M. Ambrico, M.R. Begley, E.H. Jordan, Acta Mater. 49 (2001) 1577–1588.
[7] A.M. Karlsson, J.W. Hutchinson, A.G. Evans, J. Mech. Phys. Solids 50 (2002) 1565–1590.
[8] K. Sfar, J. Aktaa, D. Munz, Mater. Sci. Eng. A333 (2002) 351–360.
[9] N. Padture, M. Gell, E. Jordan, Science 296 (2002) 280–284.
[10] M.J. Stiger, N.M. Yanar, M.G. Toppings, F.S. Pettit, G.H. Meier, Z. Metallk. 90 (1999) 1069–1082.
[11] J.A. Ruud, A. Bartz, M.P. Borom, C.A. Johnson, J. Am. Ceram. Soc. 84 (2001) 1545–1552.
[12] T. Xu, M.Y. He, A.G. Evans, Acta Mater. 51 (2003) 3807–3820.
[13] D.S. Balint, J.W. Hutchinson, J. Mech. Phys. Solids 53 (2005) 949–973.
[14] J.A. Nychka, T. Xu, D.R. Clarke, A.G. Evans, Acta Mater. 52 (2004) 2561–2568.
[15] A.W. Davis, A.G. Evans, Acta Mater. 53 (2005) 1895–1905.
[16] T. Xu, S. Faulhaber, C. Mercer, M. Maloney, A. Evans, Acta Mater. 52 (2004) 1439–1450.
[17] M.W. Chen, M.L. Glynn, R.T. Ott, T.C. Hufnagel, K.J. Hemker, Acta Mater. 51 (2003) 4279–4294.
[18] M. Maloney, private communication.
[19] D.R. Clarke, Acta Mater. 51 (2003) 1393–1407.
[20] A.H. Heuer, unpublished research.
[21] X. Chen, J.W. Hutchinson, M.Y. He, A.G. Evans, Acta Mater. 51 (2003) 2017–2030.
[22] J. Dundurs (Ed.), Mathematical Theory of Dislocations, American Society of Mechanical Engineering, New York, 1969, pp. 70–115.
[23] J.W. Hutchinson, S. Suo, Adv. Appl. Mech. 29 (1992) 64–192.
[24] F. Gaudette, S. Suresh, A.G. Evans, G. Dehm, M. Rühle, Acta Mater. 45 (1997) 3503–3514.
[25] F.G. Gaudette, S. Suresh, A.G. Evans, Metall. Mater. Trans. 31A (2000) 1977–1983.